

Comparison of Remote Sensing Algorithms for Discrimination of Major Rock Units Using ASTER Data at Lakhra Anticline, Sindh, Pakistan

Muhammad Anees*, Muaaz Shoukat, M. Akbar Khan, Mussawir Abbasi

Abstract— In this study, we have compared results of three image processing techniques; Spectral indices (SI), Featured Principal component analysis (FPCA) and Band ratio (BR) using ASTER satellite remote sensing data for lithological discrimination at Lakhra, Sindh. SI for minerals like Calcite, Dolomite, Laterite (Iron oxides) and Clay are generated using VNIR & SWIR bands, on basis of spectral absorption features of major rock forming minerals. Principal components are produced using Crosta Technique to decorrelate calcite and -OH (clay) minerals. Eigen values of PC-3 have maximum decorrelation values (0.851484 & -0.463157 in band 6 & 8) indicating presence of calcite. Also, Eigen vector values of PC-4 (-0.675364 & 0.714621) for band 5 and 6 indicate presence of -OH bearing clay minerals. Band Ratios (4/3-5/8-4/6) are used to discriminate rocks based upon their mineralogical compositions. Overall, Spectral Index method with 64% accuracy, is found to be the most effective technique among the others for lithological mapping of major rock units including carbonate (limestone, dolomite), shale (clays) & laterite (Fe oxide minerals). Comparison of satellite image processing results shows a good agreement with field samples and geological map of study area.

Index Terms—ASTER, Lakhra Anticline, Spectral Indices, Band Ratio, Featured Principal Component Analysis

I. INTRODUCTION

Exploration of natural resources and their mapping has remained one of the fundamental motivation for remote sensing scientists. The field of remote sensing has advanced rapidly with the development of strong computation algorithms and generation of rich databases [1]. At present, remote sensing and other geospatial techniques have become an essential supplementing tool for earth scientists to explore remote and large areas of earth for exploration and mapping activities [2].

ASTER (Advanced Spaceborne Thermal Emission and Reflection Radiometer), a space-borne earth observation sensor, located onboard Terra satellite, offers multispectral imagery with 15 spectral bands covering Visible-Near Infrared (VNIR), Short Wave Infrared (SWIR) and Thermal Infrared (TIR) regions of electromagnetic (EM) spectrum. Major rock forming minerals show their characteristic absorption features in SWIR region of EM spectrum [3]. ASTER has six bands in SWIR region thus offering an effective dataset for exploration of mineral resources [4-6].

Lakhra, located in Sindh province of Pakistan, is known for its extensive coal resources and lateritic clay. Massive coal mining is already being carried out in this area, while there is much more potential of coal and laterite exploration in the area which could be further exploited by using ASTER

satellite imagery. In this context, the current study focuses on learning the potential of different image processing algorithms by employing ASTER data to map different lithological units in this area. The accuracy of three image processing techniques (Spectral indices, Principal component analysis and Band ratios) have been compared with each other along with the available ground information conducted in earlier studies [7].

II. STUDY AREA AND GEOLOGICAL SETTING

Lakhra anticline is a north trending breached structure situated 40km west of Hyderabad, Sindh. The dimensions of Lakhra Anticline are 15 miles east-west and 43miles north-south (Fig. 1). Lakhra anticline was named after intermittent principal drainage system that is called Lakhra Nala. The major rock type present in the study area include limestone, shale, dolomite, sandstone and with traces of iron beds (laterite) exposed on surface [8].

Structurally, the Lakhra anticline is a part of long doubly

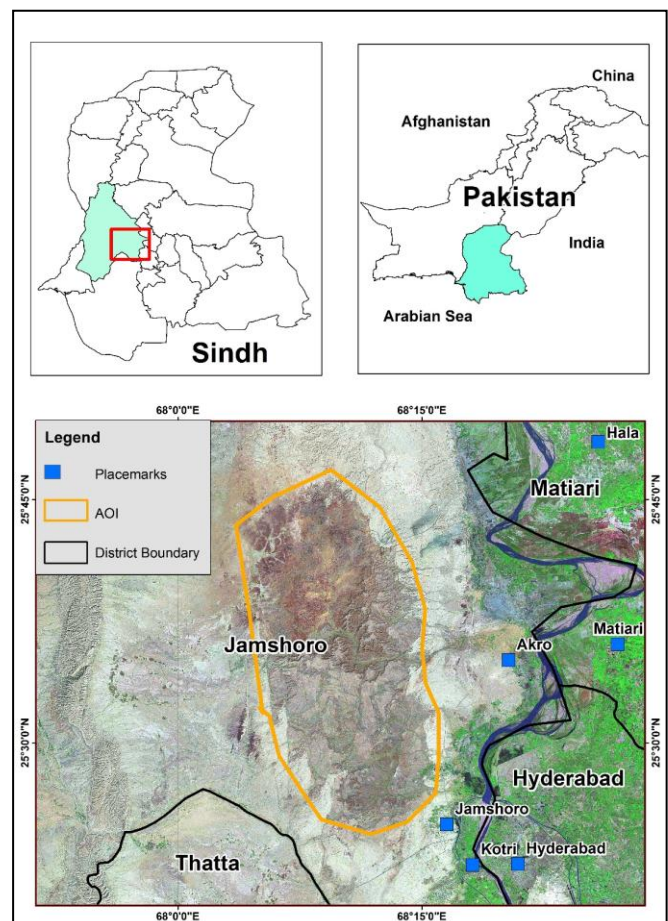


Fig. 1. Location Map of study area. Lakhra Anticline is shown by orange color boundary.

*Space Technology Applications Directorate, Space and Upper Atmospheric Research Commission, Karachi, Pakistan
Corresponding Author: muhammad.anees.pk@gmail.com

plunging anticline, which runs North-South direction. Rocks of Paleocene Ranikot group are exposed in this area which is divided into Khaskheli Basalts, Khadro Formation, Bara Formation and Lakhra Formation [8]. The Bara Formation (Middle Paleocene) is the oldest Formation and occurs in the core of the Lakhra anticline, whereas the Laki Formation is the youngest Formation of this area and occurs on the flanks of the Lakhra anticline. Bara Formation is composed of sandstone which is multicolored, fine to coarse grained, soft, crumbly, and poorly sorted. It is laminated to massive, calcareous, ferruginous, ripple marked and cross-bedded. The sandy, soft, carbonaceous and gypsiferous shales are grey, yellowish green and multicolored and contains coal [9]. Lakhra Formation mainly comprises of clastic sediments of shallow-marine environment such as; claystone, siltstone and argillaceous fine grained sandstone. Lakhra Formation has a conformable contact with underlying coal-bearing Bara Formation. Lakhra Formation is unconformable overlain by Sohnari member (coal-bearing) of Laki Formation [10]. Figure 2 presents the detailed geological map of the study area. The stratigraphy of the Lakhra anticline is tabulated in Table 1.

The area contains deposits of limestone, coal and minor occurrence of gypsum. Limestone of this area is a good source for cement factory, construction and ornamental purposes. Gypsum occur as lenticular lenses in shale of Lakhra Formation belonging to upper Paleocene age [11]. Bituminous type of coal is present in Lakhra Formation and is being mined locally. This coal is used for the various purposes in the industries.

TABLE 1. Stratigraphic Sequence of the study area (after Shah, 2009)

III. METHODOLOGY

A. Pre-Processing

The study used ASTER L1B data which is downloaded free of charge from United States Geological Survey (USGS) Earth Explorer (<http://earthexplorer.usgs.gov>). ASTER Level 1B is being offered by USGS with pre-corrected geometric and radiometric errors. VNIR bands of ASTER have spatial resolution of 15m whereas, SWIR bands have a spatial resolution of 30m. Prior to application of image processing algorithms, VNIR bands have been resampled to 30m and stacked with SWIR bands. The resultant file comprises of 9 ASTER VNIR-SWIR bands of 30m spatial resolution. Fast Line-of-sight Atmospheric Analysis of Spectral Hyper-cubes (FLAASH) model [12], available in ENVI 4.8 (Environment for Visualizing Images Software) is used for atmospheric correction of data. The FLAASH model requires several parameters as input from metadata file available along satellite image to remove atmospheric influence and converts top of atmosphere radiance into surface reflectance.

B. Band Ratios

Band ratio is a simple technique to limit the spectral divergence in an image by dividing a band by another [13]. Band ratios to delineate spatial distribution of specific lithological units are adopted after Kalinowski and Oliver, 2004 by analyzing the spectral response of major rocks present in the area. Spectral reflectance of rocks is the key signature in remote sensing based geological mapping. Since, Limestone, Laterite and shale are main rock types in study area, their spectral characteristics form the basis for

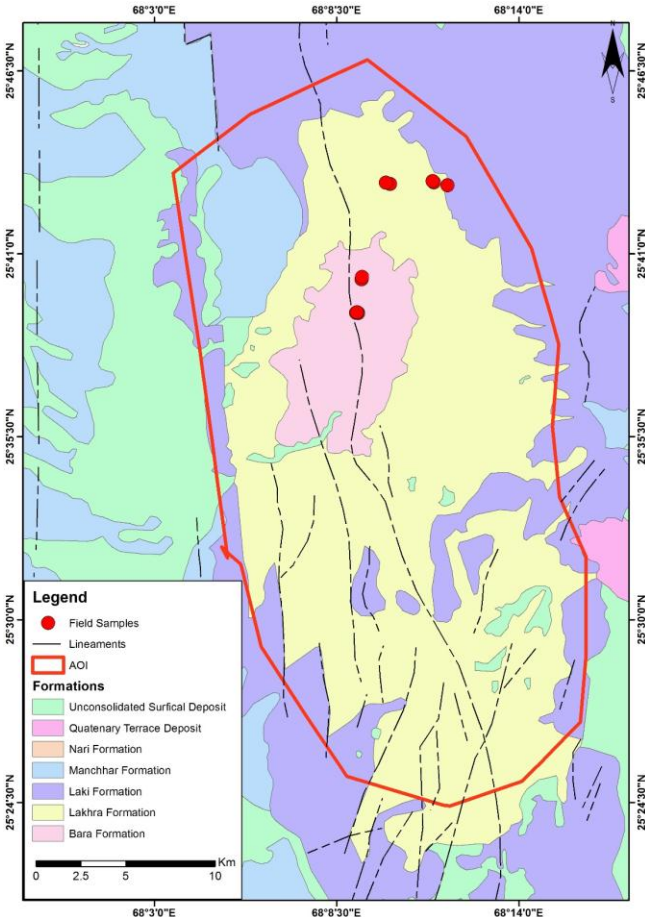


Fig. 2. Geological Map of study area (after Outerbridge et. Al., 2007).

Age	Group	Formation	Major Lithology
Miocene		Manchar Formation	Sandstone, shale, clay with subordinate conglomerates
Eocene		Laki Formation	Limestone, calcareous shale, sandstone, laterite
Paleocene	Ranikot Group	Lakhra Formation	Limestone, Sandstone, shale interbeds
		Bara Formation	Sandstone, shale
		Khaddro Formation	Sandstone, shale, basaltic flows

selection of band ratios (Fig. 4). The three band ratios are applied in the study include: 5/8 for identifying calcite rich rocks (carbonate); 4/3 for rocks with iron oxide (laterite); and 4/6 for rocks with major clay (shale) [14].

C. Principal Component Analysis

Principal Component Analysis (PCA) is a multivariate statistical based approach which was first introduced by Pearson (1901). PCA is based on mathematical calculation which utilizes orthogonal transformation of coefficients for conversion of correlated variable into uncorrelated variables, Principal Component Analysis reduces the dimensionality of data set in a way that the total number of PCs are less than or equal to original number of variables [15].

The variance in statistics of PC bands is associated with the response of various surficial materials to EM light and the dimensionality of image data [16].

PCA for ASTER data are produced based on spectral response of rocks in different wavelengths of electromagnetic spectrum [16-18]. The FPCA or Crosta method comprises of selection of spectral subset to enhance the decorrelation for indented material (rocks, vegetation, soil etc.). Since specific bands are used, the interpretation of resultant imagery becomes much easier in FPCA than PCA.

D. Spectral Indices

Spectral Indices involves orthogonal transformation of multispectral data with a pre-defined transform axis for representation of a certain pattern. Since, spectral indices use pre-defined coefficients, it is much easier to interpret and extract to certain degree the physical meaning of transformed resultant image from geological point of view [19, 20].

As the study area is predominantly covered with sand, clay with minor limestone on the periphery and ferrous oxidation at some parts, the spectral indices are adopted after Yamaguchi and Naito, 2003 to find rock distribution on ASTER imagery. Clay Index, Calcite Index, Ferrous Ion Index are used based on spectral response of rock types towards different portions of electromagnetic spectrum [21].

The characteristic absorption feature for calcite mineral is marked at band 8 of ASTER data. Similarly, calcite mineral shows high reflectance value at band 6 and 9 [20]. Calcite Index (CI) is shown in equation (1).

$$C.I = \text{Band 6} \times \text{Band 9} / \text{Band 8} \times \text{Band 8} \quad (1)$$

The absorption in Hydroxyl minerals (clays) is caused by the presence of aluminum hydroxide (Al-OH) bond and can be mapped through using Hydroxyl Index (H.I) which is shown in equation 2 [22].

$$H.I = \text{Band 4} \times \text{Band 7} / \text{Band 6} \times \text{Band 6} \quad (2)$$

Iron oxide minerals such as hematite has absorption at near infrared corresponding to band 3 of ASTER data and can be identified using Ferrous Index (FI) as shown in

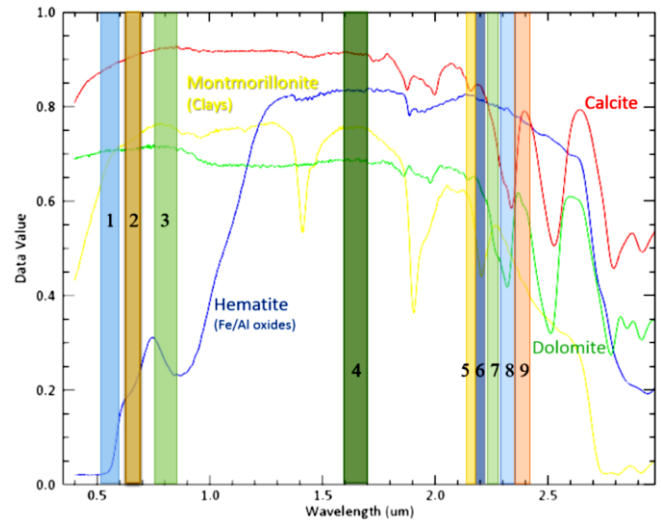


Fig. 4. Availability of ASTER VNIR-SWIR bands 1-9 relative to spectra of common minerals of the study area (after USGS Spec Lib 6, 2007).

Equation 3 [14, 23].

$$F.I = \text{Band 5} / \text{Band 3} + \text{Band 1} / \text{Band 2} \quad (3)$$

IV. RESULTS AND DISCUSSION

Results of band ratios in Fig. 5 show the false color composite of band ratio of 5/8, 4/3 and 4/6, which are calculated from ASTER surface reflectance data. BR 5/8 indicates carbonates in the light bluish green color distributed mostly in the center and outer rim of the area (Fig. 5). Montmorillonite, Alunite, Kaolinite and other alteration / clay minerals are associated with argillaceous rocks (shale). These alteration minerals are highlighted towards southern parts of the area in light to dark blue color by band ratio 4/6 (Fig. 5). Iron oxide minerals such as hematite are formed in oxidation conditions and are mostly associated with surface weathering (laterite). BR 4/3 highlights the distribution of iron oxides in the northern areas in light pink to red color (Fig. 5).

Out of four PC bands extracted form PCA of ASTER bands, PC-1 contains maximum information around 95% and shows correlated features, while PC-4 has minimum information but shows high decorrelation. For this reason, only decorrelated bands (PC-3 and PC-4) are selected and analyzed for discrimination of lithological units. Eigenvalues of four PC bands generated from ASTER bands 3, 6, 8 & 9 are shown in Table 2. The response of each PC band is compared to the geological map representing major lithologies. PC-3 band is found to be true representation of calcite as it has positive value for band 6 and negative eigenvalue for band 4 (Table 2). Eigenvalues of four PC bands generated from PCA of ASTER bands 1, 3, 5 & 6 are shown in Table 3. PC-4 band shows a positive eigenvalue for band 6 and a negative eigenvalue for band 5 (Table 3) and is selected to delineate clay minerals in the image (Fig. 6). For iron oxide minerals (laterite), PC-4 from PCA of ASTER bands 1, 2, 3 & 4 is selected. False color composite (FCC) image (Fig. 6) is produced using PC bands from PCA of 3689 (PC-3), 1356 (PC-4) & 1234 (PC-4) to discriminate and highlight limestone, shale and laterite respectively. In Fig. 6, Carbonates (containing calcite & dolomite) are highlighted in dark to light blue, shales (clay) in orange to yellow tones, and laterites (iron oxides) in purple to pinkish colors.

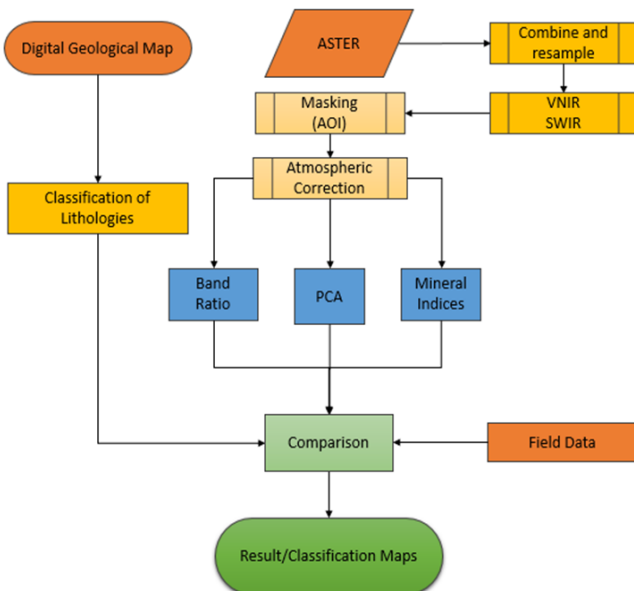


Fig. 3. Methodological Flow chart of the study

Fig. 7 shows results of spectral indices of CI (Calcite), HI (Clays) and FI (Iron oxides) with a thematic map which is produced by extracting and coloring pixel values of 230-255 (CI; Green), 181-244 (HI; Yellow), and 201-255 (FI; Red) respectively. High values CI (>230) indicates presence of carbonate minerals, calcite and dolomite [24]. Rocks with high CI are mostly distributed around the flanks of anticline (Fig. 7) coinciding with limestone of Laki formation (Fig. 8). Distribution of HI values (181-244) show the presence of clay minerals which can be inferred as shales (Fig. 7). As the Lakhra formation is predominantly composed of Argillaceous limestone along with shale and sandstone, the spatial distribution of high values of HI seems to agree with the geological map (Fig. 8). FI with values >201 indicates occurrence of iron oxide minerals such as hematite which are associate with laterites and oxidized sandstones [25, 26]. According to geological map, Bara and Manchhar formations are composed of ferruginous sandstones and shales (Fig. 8). Distribution of high values of FI overlaps with locations of these two geological units (Fig. 7).

TABLE 2. Eigen values of FCPA of ASTER bands 3, 6, 8 & 9

PC	Band 3	Band 6	Band 8	Band 9
1	-0.423338	-0.470681	-0.439735	-0.637085
2	-0.850627	-0.065385	0.394751	0.341072
3	0.287072	-0.625548	0.694917	-0.208252
4	0.121689	-0.618768	-0.409750	0.659108

TABLE 3. Eigen values of FCPA of ASTER bands 1, 3, 5 & 6

PC	Band 1	Band 3	Band 5	Band 6
1	-0.310049	-0.509883	-0.568793	-0.566006
2	-0.521134	-0.612582	0.465127	0.369892
3	0.776639	-0.600568	-0.063362	0.179261
4	-0.170647	0.063880	-0.675364	0.714621

Results of all three image processing algorithms used in the study are compared with geological map and field samples collected from the area (Fig. 8). The data used for referencing and validation comprised of 14 ground samples of limestone, shale, sandstone and laterite. Due to this limited ground data and geological map, only a qualitative comparison could be performed [27]. Table 4 shows a comparison of the image processing results with the ground based referenced data from 14 locations (Fig. 5, Fig. 6, Fig

7 & Fig. 8). Among all algorithms used in the research, SI proved to be most viable method for discrimination of carbonates minerals including limestone and dolomite with accuracy of 64%. Whereas, PCA with 42% accuracy is the regarded as supplementary technique for differentiating (decorrelation) distinct boundaries between rock types (Fig. 6).BR method although seems to be less accurate (35%), but it still has been effective in delineating iron oxide rich zones (Fig. 5).

Although results proved effective in discriminating major lithological units present in the area, however at some regions where intermixing of units have occurred, a clear discrimination could not be achieved. As the 30m spatial resolution data is used in the study, localized units with less lateral distribution posed problems in discrimination due to spectral mixing of multiple minerals at pixel level. This effect is dominant where weathering and mining activities have disturbed the surface cover of the area. To overcome these limitations and for better mapping, potentials of high spatial and spectral resolution airborne and satellite sensors, such WorldView-3 and AVIRIS may be exploited.

V. CONCLUSION

This study has qualitatively analyzed the results of remote sensing algorithms to discriminate and identify different sedimentary rocks / minerals at the study area. ASTER imagery due to its good spatial and spectral coverage offered discrimination and identification of rock units within geological formations. Spectral Indices, Principal Component Analysis (Crosta method) and Band Ratio are used and proved effective in discriminating rocks & surface minerals. All techniques were able to discriminate rocks and minerals in study area up to some extent. Overall, Spectral indices successfully discriminated all major rocks and surface minerals (Carbonates, Shale/Clays and Laterite/Iron oxides) on the basis of their spectral responses. Classifications based upon spectral indices, are in good agreement (64%) with earlier studies and geological maps. Whereas, PCA successfully identified limestone and shale but could not discriminate clearly between clays and iron oxides. Band ratio method is simpler than the SI and PCA method, however, its results are somewhat coarse and not as reliable as that of other two methods. This study shows that SI method could be more suitable for detection and discrimination of sedimentary rocks and minerals in the arid area.

TABLE 4. Comparison of results generated through image processing algorithms with geological map classification and ground samples

S. No.	Geographic Coordinates	Field Sample	Geological Map	Results		
				SI	PCA	BR
1	68.1540 E 25.6705 N	Shale	Bara Fm	Clay/FeO	Clay	Laterite
2	68.1514 E 25.6537 N	Laterite	Lakhra/Bara Fm	FeO/Clay	Clay	Clay
3	68.1523 E 25.6535 N	Laterite	Bara Fm	FeO/Clay	Clay	Clay
4	68.1519 E 25.6540 N	Sandstone	Bara Fm	Clay/FeO	Laterite	Laterite
5	68.1684 E 25.7183 N	Alluvium	Surficial Deposits	Laterite	Clay/ Laterite	Laterite
6	68.1972 E 25.7177 N	Limestone/Laterite	Lakhra/Laki Fm	Calcite/ Laterite	Calcite/Clay	Laterite
7	68.1905 E 25.7191 N	Limestone	Lakhra Fm	Clay/ Calcite	Clay	Clay
8	68.1684 E 25.7183 N	Limestone	Lakhra Fm	Calcite/ Laterite	Clay	Laterite
9	68.1662 E 25.7189 N	Limestone	Lakhra Fm	Laterite/Calcite	Laterite	Clay/ Laterite
10	68.1898 E 25.7197 N	Limestone	Lakhra Fm	Clay/ Calcite	Clay	Laterite
11	68.1519 E 25.6545 N	Limestone	Lakhra Fm	Clay/ Calcite	Clay	Clay
12	68.1541 E 25.6706 N	Sandstone	Bara Fm	FeO/Clay	Laterite	Laterite
13	68.1517 E 25.6539 N	Limestone	Lakhra Fm	Clay	Clay	Clay
14	68.1543 E 25.6717 N	Shale	Lakhra/Bara Fm	Clay	Clay	Clay
Matched =				64	42	35
Mismatched =						
Accuracy (%)				64	42	35

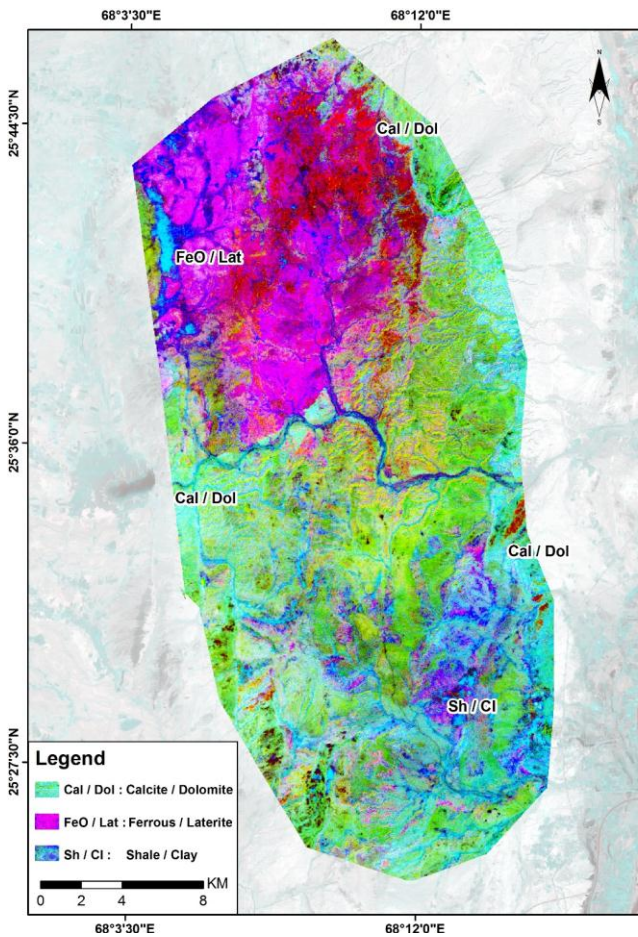


Fig. 5. FCC image of band ratio 4/3(R), 5/8(G), 4/6(B) showing distribution of Calcite/Dolomite, Shale/Clay and Ferrous/Laterite in study area.

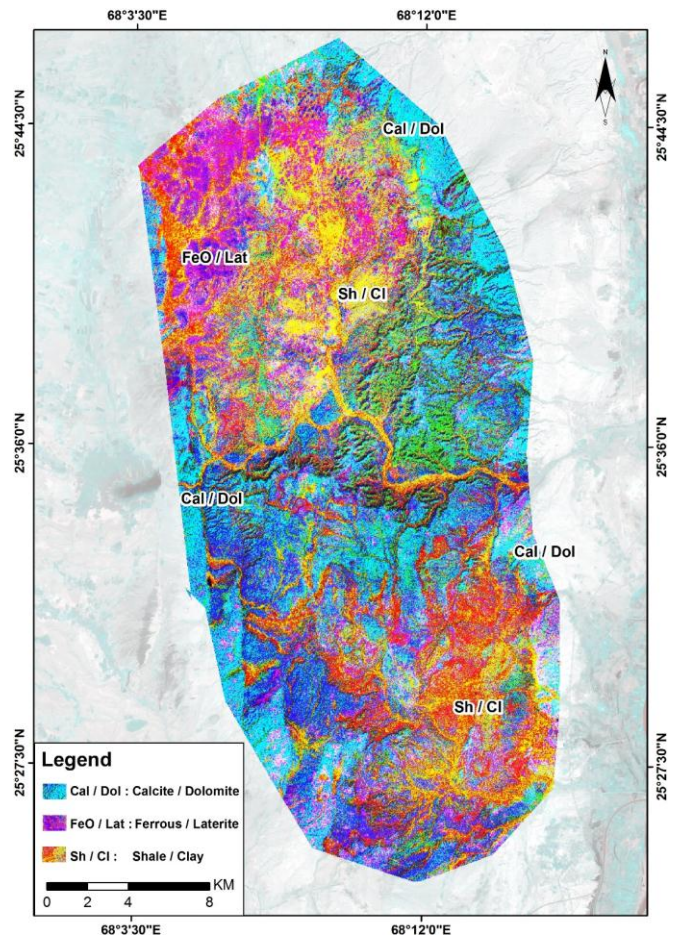


Fig. 6. FCC image of FPCA of 3678 (PC-3), 1356 (PC-4) & 1234 (PC-4)

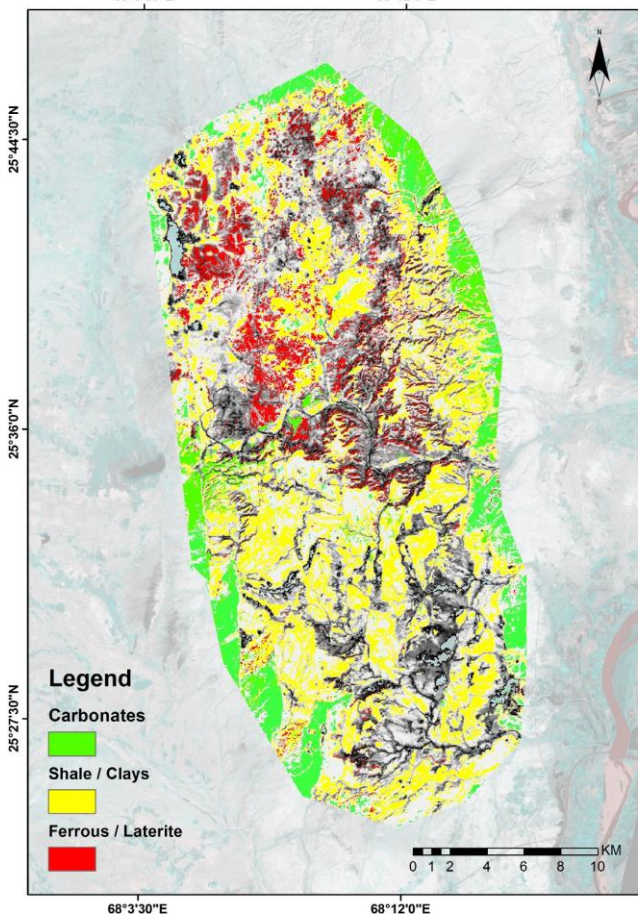


Fig.7. Spectral indices of Calcite, clay and ferrous minerals.

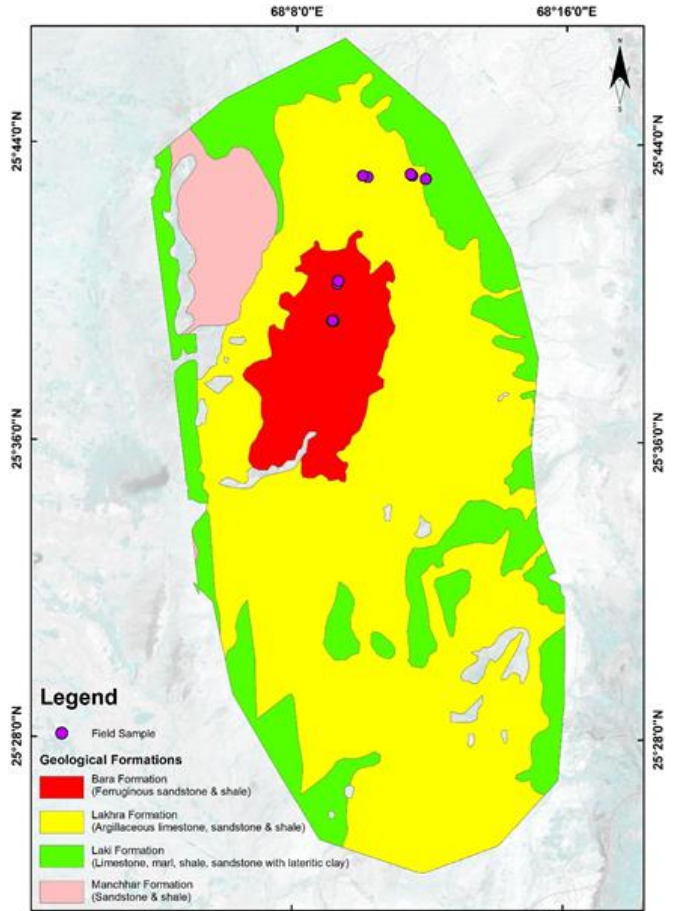


Fig.8. Digitized Geological Map of study area showing major lithologies along with location of rocks samples collected from field.

VI. ACKNOWLEDGMENTS

Authors would like to acknowledge Mr. Muhammad Arsalan (Lecturer, Department of Geology, University of Karachi) for sharing the results of his field study conducted at the study area.

REFERENCES

- [1] R. G. Congalton, "A review of assessing the accuracy of classifications of remotely sensed data," *Remote sensing of environment*, vol. 37, no. 1, pp. 35-46, 1991.
- [2] R. P. Gupta, *Remote sensing geology*. Springer Science & Business Media, 2013.
- [3] M. Abrams and S. J. Hook, "Simulated ASTER data for geologic studies," *IEEE Transactions on Geoscience and remote sensing*, vol. 33, no. 3, pp. 692-699, 1995.
- [4] L. C. Rowan and J. C. Mars, "Lithologic mapping in the Mountain Pass, California area using advanced spaceborne thermal emission and reflection radiometer (ASTER) data," *Remote sensing of Environment*, vol. 84, no. 3, pp. 350-366, 2003.
- [5] X. Zhang, M. Pazner, and N. Duke, "Lithologic and mineral information extraction for gold exploration using ASTER data in the south Chocolate Mountains (California)," *ISPRS Journal of Photogrammetry and Remote Sensing*, vol. 62, no. 4, pp. 271-282, 2007.
- [6] F. D. Van der Meer *et al.*, "Multi-and hyperspectral geologic remote sensing: A review," *International Journal of Applied Earth Observation and Geoinformation*, vol. 14, no. 1, pp. 112-128, 2012.
- [7] W. F. Outerbridge, J. R. SanFilipo, and R. A. Khan, "The Lakhra Anticline-An Active Structure of Pleistocene to Holocene Age in Southern Pakistan," Geological Survey (US)2328-0328, 2007.
- [8] S. M. I. Shah, *Stratigraphy of Pakistan*. Govt. of Pakistan Ministry of Petroleum & Natural Resorces, Geological Survey of Pakistan, 2009.
- [9] A. D. HAKRO and M. Baig, "Depositional environment of the Bara formation, fort ranikot area, Sindh," *Sindh University Research Journal-SURJ (Science Series)*, vol. 45, no. 1, 2013.
- [10] S. F. Fatmi and I. A. Khan, "A guide to Stratigraphy of Sindh," Geological Survey of Pakistan, Information Release 1995, vol. 558.
- [11] I. Brohi *et al.*, "Joint analysis and economic significance of Lakhra Formation in the vicinity of Khanu Brohi, Jamshoro, Sindh," *Sindh University Research Journal-SURJ (Science Series)*, vol. 45, no. 2, 2013.
- [12] S. Adler-Golden *et al.*, "FLAASH, A MODTRAN4 atmospheric correction package for hyperspectral data retrievals and simulations," in *Proc. 7th Ann. JPL Airborne Earth Science Workshop*, 1998, vol. 97, pp. 9-14: JPL Publication Pasadena, CA.
- [13] T. M. Lillesand and R. W. Kiefer, "chipman, JW 2004. Remote Sensing and Image Interpretation," ed: John wiley & Sons, New York, USA.
- [14] A. Kalinowski and S. Oliver, "ASTER mineral index processing manual: Remote Sensing Applications," Geoscience Australia2004.
- [15] A. Singh, "Review article digital change detection techniques using remotely-sensed data," *International journal of remote sensing*, vol. 10, no. 6, pp. 989-1003, 1989.
- [16] W. Loughlin, "Principal component analysis for alteration mapping," *Photogrammetric Engineering and Remote Sensing*, vol. 57, no. 9, pp. 1163-1169, 1991.
- [17] A. P. Crosta and J. M. MOORE, "Geological mapping using Landsat thematic mapper imagery in Almeria Province, south-east Spain," *International Journal of Remote Sensing*, vol. 10, no. 3, pp. 505-514, 1989.
- [18] A. Crosta, C. De Souza Filho, F. Azevedo, and C. Brodie, "Targeting key alteration minerals in epithermal deposits in Patagonia, Argentina, using ASTER imagery and principal component analysis," *International journal of Remote sensing*, vol. 24, no. 21, pp. 4233-4240, 2003.
- [19] E. P. Crist and R. C. Cicone, "A physically-based transformation of Thematic Mapper data---The TM Tasseled Cap," *IEEE Transactions on Geoscience and Remote sensing*, no. 3, pp. 256-263, 1984.
- [20] Y. Yamaguchi and C. Naito, "Spectral indices for lithologic discrimination and mapping by using the ASTER SWIR bands," *International Journal of Remote Sensing*, vol. 24, no. 22, pp. 4311-4323, 2003.
- [21] N. S. Oztan and M. L. Suzen, "Evaporate mapping in Bala region (Ankara) by remote sensing techniques," in *4th International Conference on Recent Advances in Space Technologies*, 2009, pp. 39-42: IEEE.
- [22] A. B. Pour and M. Hashim, "The application of ASTER remote sensing data to porphyry copper and epithermal gold deposits," *Ore Geology Reviews*, vol. 44, pp. 1-9, 2012.
- [23] R. N. Clark *et al.*, "USGS digital spectral library splib06a," *US geological survey, digital data series*, vol. 231, 2007.
- [24] G. R. Hunt and J. W. Salisbury, "Visible and near infrared spectra of minerals and rocks. II. Carbonates," *Modern Geology*, vol. 2, pp. 23-30, 1971.
- [25] M. Andrews Deller, "Facies discrimination in laterites using Landsat Thematic Mapper, ASTER and ALI data---examples from Eritrea and Arabia," *International Journal of Remote Sensing*, vol. 27, no. 12, pp. 2389-2409, 2006.
- [26] S. Salem, "ASD field hyperspectral measurements for discrimination of the ferruginous rocks and the iron ore types at El Gedida-Ghorabi area, Bahariya Oasis, Western Desert, Egypt," *Arabian Journal of Geosciences*, vol. 10, no. 7, p. 166, 2017.
- [27] Y. Ninomiya, "Rock type mapping with indices defined for multispectral thermal infrared ASTER data: case studies," in *Proceedings of SPIE*, 2003, vol. 4886, pp. 123-132.